Vibration Model to Detect Local Defect Characteristics of Deep Groove Ball Bearing

Ajay Kumar Verma
Shivalik College of Engineering

Parveen Kumar Saini
National Institute of Technology

https://doi.org/10.5109/6625791

出版情報：Evergreen. 9 (4), pp.1056-1066, 2022-12. 九州大学グリーンテクノロジー研究教育センター
バージョン：

Vibration Model to Detect Local Defect Characteristics of Deep Groove Ball Bearing

Ajay Kumar Verma[1,*], Parveen Kumar Saini[2]
[1]Shivalik College of Engineering, Dehradun, Indian
[2]National Institute of Technology, Kurukshetra, India

*Author to whom correspondence should be addressed:
E-mail: ajayverma84114@gmail.com

(Received September 26, 2022; Revised November 14, 2022; accepted November 21, 2022).

Abstract: The vibration model, to analyze the local defect in the deep groove ball bearing system is reported in this paper. Shaft, races, balls, and housing masses along with damping at the ball-race interface and defects on its races are considered in the model. The governing equations are solved using MATLAB to simulate the vibration responses of the bearing system. To validate the simulation results, experiments have been performed and compared with simulated results. The comparison shows that the simulated characteristic frequencies differ with experimental values between 0.19 % to 0.72 % which is negligible. The velocity amplitudes at characteristic frequencies in simulated results are in poor agreement with experimental values. This is due to the defects like misalignment, residual unbalancing, etc. are ignored in the theoretical model. Since the simulated results are depicting the same characteristics as it is shown in experimental results, therefore, this vibration model can be used to study the vibration characteristics and to predict the localized defects in ball bearings.

Keywords: Deep groove ball bearing, bearing defects, vibration model, bearing mechanics, bearing analysis.

1. Introduction

Vibration analysis technique to detect local defects in rolling element bearing is widely used due to its prompt response. The intensive research studies carried out by several researchers are discussed here. Researchers[1-5] have proposed a dynamic model with 2-DOF using Hertzian contact theory. Tandon and Chaudhary[6], have suggested the frequency and amplitude prediction model analytically for bearing with local defects. Tiwari et al.[7-8] have suggested that the non-linearity characteristics of a rotor system increase with an increment in bearing clearance. Feng et al.[9] have included the effect of cage and ball slip over the races in their model with 2-DOF. Chaudhary and Tandon[10] have used lumped masses phenomena for shaft and housing and considered linearized stiffness to propose the dynamic model for bearing with defects. Kiral and Karagulle[11] have considered more than one defect and variable defect positions in their model. Cong et al.[12] have included the defect location and unbalancing of the rotor system in their studies. Arslan and Akturk[13] have proposed dynamic model with ball deformation. Brie[14] has done the theoretical study and discussed the spalled bearing problems. Tandon and Nakra[15] have done experimental vibration studies to identify the defect frequencies for defective bearings. Tandon[16] has suggested that the capability of power is better than the peak and RMS measurement in his studies of defect detection parameters. Ashtekar et al.[17] have developed the vibration model to analyze the effects of defects on rolling bearing. The authors have concluded that a single defect can affect the motion and forces on all components of the bearing.

Sopanen and Mikkola[18-19] presented the dynamic model for rolling bearing system considering 6-DOF with surface waviness and localized defects. The authors have considered the Hertzian contact theory and elatohydrodynamic lubrication. The mass of housing and shaft mass were ignored in this model. Wijnant et al.[20] have introduced elastohydrodynamic lubrication theory into their model for rolling element bearing. Babu et al.[21] have proposed a vibration model for angular contact bearing and considered the frictional moments in the bearings including the waviness of surfaces of bearing elements. Authors have considered the presence of lubricating film and Hertzian deformation as a major source of damping calculation and included the elastohydrodynamic lubrication theory to calculate ball deformation. Yu et al.[22] have presented a mathematical model based on 4-DOF to extract vibration features of deep groove ball bearing but the authors have not

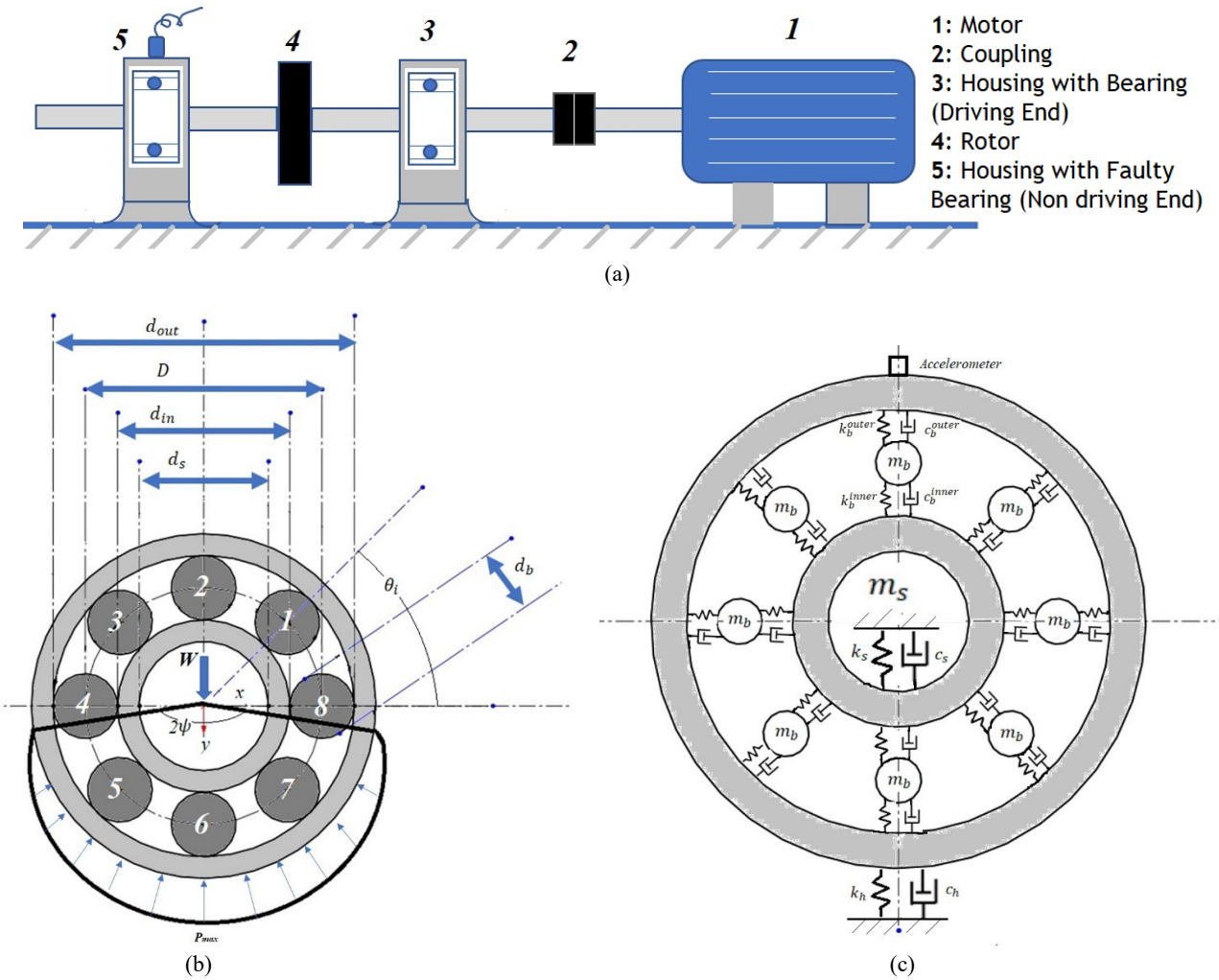

Fig. 1: The system of bearing used for study: (a) test setup, (b) bearing nomenclature and load distribution (c) bearing components and the free body diagram

modeled any defect available on the elements of the bearing. Hou et al.[23] have proposed a nonlinear vibration model for ball bearing considering the distributed defects present on the surface of its elements and concluded that the distributed defects of specific order produce the characteristic frequency which is proportional to the speed of rotation. Though the authors have considered distributed defects, they ignored the presence of local defects in their model. Researchers[24-26] have established a vibration model to analyze the characteristic frequency for bearing with localized defects but the authors have ignored the effects of damping present in the bearing.

The aim of this paper is to propose a comprehensive and accurate vibration model to analyze the local defects in the deep groove ball-bearing system. The shaft, races, balls, and housing masses including the effect of damping at the ball-race interface along with defects on races have been incorporated into the model. To validate the simulation results, experiments have been performed and compared with simulated results. The comparison shows that the simulated results are depicting the same characteristics as it is shown in experimental results.

2. Vibration modeling of ball bearing

A 6-DOF system is considered to develop a nonlinear vibration model for deep groove ball bearing. The system of bearing considered for the study is shown in Fig. 1(a). Fig. 1(b) shows the load distribution and nomenclature of bearing. The free body diagram of bearing is shown in Fig. 1(c).

The angular position of i^{th} ball θ_i at time t can be given by the relation

$$\theta_i = \frac{2\pi i}{n_b} + \omega_{cage} t + \theta_0 \qquad (1)$$

where the angular position of i^{th} ball from x-axis is taken as θ_0. The cage velocity is expressed as,

$$\omega_{cage} = \omega_s \times \left(1 - \frac{d_b}{D}\right) \quad (2)$$

2.1 Governing equations of motion

Analyzing the free body diagram of bearing system Fig. 2, the differential equations of motion are derived as:

For shaft and inner race, the differential equations of motion along x-axis and y-axis are given as:

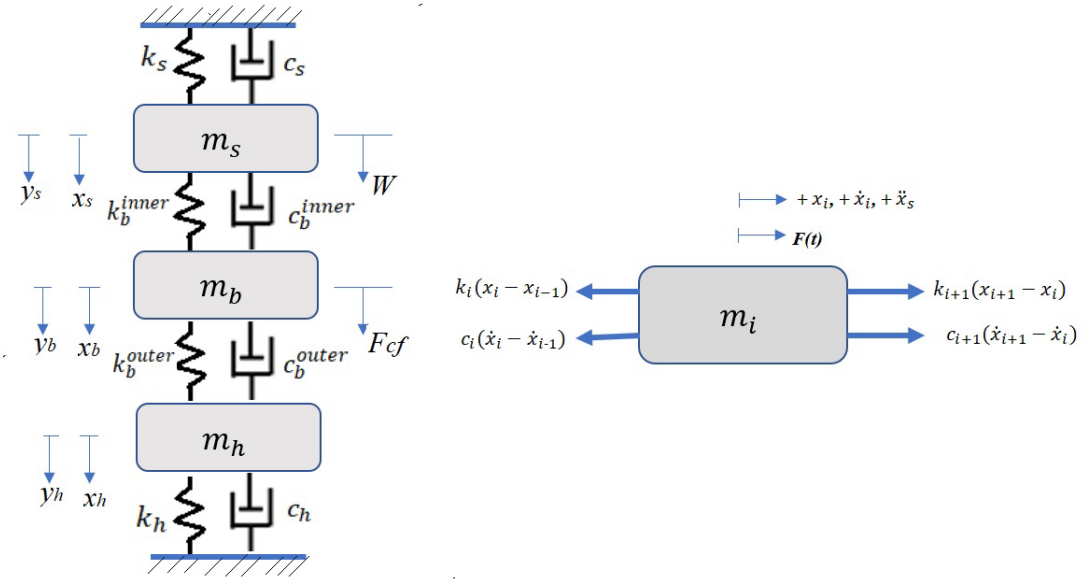

Fig. 2: The free-body diagram of bearing system

$$m_s\ddot{x}_s + c_s\dot{x}_s + k_s x_s + f_{cx}^{inner} + f_{dx}^{inner} = 0 \quad (3)$$

$$m_s\ddot{y}_s + c_s\dot{y}_s + k_s y_s + f_{cy}^{inner} + f_{dy}^{inner} = W \quad (4)$$

For ball, the differential equations of motion along x-axis and y-axis are given as:

For *1st* ball

$$m_b\ddot{x}_{b1} - f_{c1}^{inner}cos\theta_1 - f_{d1}^{inner}cos\theta_1 + f_{c1}^{outer}cos\theta_1 + f_{d1}^{outer}cos\theta_1 = 0$$

$$m_b\ddot{y}_{b1} - f_{c1}^{inner}sin\theta_1 - f_{d1}^{inner}sin\theta_1 + f_{c1}^{outer}sin\theta_1 + f_{d1}^{outer}sin\theta_1 = 0$$

For *2nd* ball

$$m_b\ddot{x}_{b2} - f_{c2}^{inner}cos\theta_2 - f_{d2}^{inner}cos\theta_2 + f_{c2}^{outer}cos\theta_2 + f_{d2}^{outer}cos\theta_2 = 0$$

$$m_b\ddot{y}_{b2} - f_{c2}^{inner}sin\theta_2 - f_{d2}^{inner}sin\theta_2 + f_{c2}^{outer}sin\theta_2 + f_{d2}^{outer}sin\theta_2 = 0$$

For *ith* ball

$$m_b\ddot{x}_{bi} - f_{ci}^{inner}cos\theta_i - f_{di}^{inner}cos\theta_i + f_{ci}^{outer}cos\theta_i + f_{di}^{outer}cos\theta_i = 0 \quad (5)$$

$$m_b\ddot{y}_{bi} - f_{ci}^{inner}sin\theta_i - f_{di}^{inner}sin\theta_i + f_{ci}^{outer}sin\theta_i + f_{di}^{outer}sin\theta_i = 0 \quad (6)$$

For housing and outer race, the differential equations of motion along x-axis and y-axis are given as:

$$m_h\ddot{x}_h + c_h\dot{x}_h + k_h x_h - f_{cx}^{outer} - f_{dx}^{outer} = 0 \quad (7)$$

$$m_h\ddot{y}_h + c_h\dot{y}_h + k_h y_h - f_{cy}^{outer} - f_{dy}^{outer} = 0 \quad (8)$$

2.2 Contacting forces

According to Hertzian contact theory, the elastic ball deformation is caused by the force,

$$f_{ci} = k_b\delta_i^{1.5} \quad (9)$$

and contacting force due to damping present at ball and races is expressed as:

$$f_{di} = c_b\dot{\delta}_i \quad (10)$$

for *ith* ball contacting forces on inner and outer race are given by,

$$f_{ci}^{inner} = \Lambda_i k_b^{inner}\left(\delta_i^{inner}\right)^{1.5} \quad (11)$$

$$f_{ci}^{outer} = \Lambda_i k_b^{outer}(\delta_i^{outer})^{1.5} \quad (12)$$

contacting forces resolved in x-direction and y-direction are given by,

$$f_{cx}^{inner} = \sum_1^{n_b}\Lambda_i\left[k_b^{inner}\left(\delta_i^{inner}\right)^{1.5}cos\theta_i\right] \quad (13)$$

$$f_{cy}^{outer} = \sum_1^{n_b}\Lambda_i[k_b^{outer}(\delta_i^{outer})^{1.5}sin\theta_i] \quad (14)$$

$$f_{di}^{inner} = \Lambda_i c_b^{inner}\left(\dot{\delta}_i^{inner}\right) \quad (15)$$

$$f_{di}^{outer} = \Lambda_i c_b^{outer}\left(\dot{\delta}_i^{outer}\right) \quad (16)$$

$$f_{dx}^{inner} = \sum_1^{n_b} \Lambda_i\left[c_b^{inner}\left(\dot{\delta}_i^{inner}\right) cos\theta_i\right] \quad (17)$$

$$f_{dy}^{outer} = \sum_1^{n_b} \Lambda_i\left[c_b^{outer}\left(\dot{\delta}_i^{outer}\right) sin\theta_i\right] \quad (18)$$

The Hertzian contacting forces will only be in action in action when balls are being deformed in loading zone[27]. Otherwise, it will be zero. To incorporate the condition a switch function Λ_i is introduced.

were,

$$\Lambda_i = \begin{cases} 1, & \text{if } \delta_i \text{ is } +\text{ve (i.e. ball is in loading zone)} \\ 0, & otherwise \end{cases} \quad (19)$$

2.3 Stiffness at ball-race interface

Based on the classical theory of elasticity and the simplified parameters given by Brewe and Hamrock[28] considering the maximum ball deformation, the contact stiffness is given by

$$k_b = \pi\kappa E' \sqrt{\left[\frac{\epsilon}{4.5(\sum\rho)\Im^3}\right]} \quad (20)$$

were,

$$\frac{1}{E'} = \frac{1}{2}\left(\frac{1-\nu_1^2}{E_1} + \frac{1-\nu_2^2}{E_2}\right) \quad (21)$$

$$\kappa = 1.0339\left(\frac{R_y}{R_x}\right)^{o.6360} \quad (22)$$

$$\epsilon = 1.0003 + \frac{0.6023}{\left(R_y/R_x\right)} \quad (23)$$

$$\Im = 1.5277 + 0.6023\, ln\left(R_y/R_x\right) \quad (24)$$

where, R_y and R_x are groove curvatures along y-axis and x-axis.

Being a function of curvature sum ($\sum\rho$), the value of contact stiffness is different at inner race and outer race because the radius of curvature differs for inner and outer races[29]. These expressions are given by

$$k_b^{inner} = \pi\kappa_{in}E'_{in}\sqrt{\left[\frac{\epsilon_{in}}{4.5(\sum\rho)_{in}\Im_{in}^3}\right]} \quad (25)$$

$$k_b^{outer} = \pi\kappa_{out}E'_{out}\sqrt{\left[\frac{\epsilon_{out}}{4.5(\sum\rho)_{out}\Im_{out}^3}\right]} \quad (26)$$

2.4 Coefficient of damping

As lubricant is provided at ball race interface for friction and wear reduction, a lubricant film is generated due to high pressure. This pressure deforms the balls in loading zone. To calculate damping coefficient, c_{ehl} due to elastohydrodynamic lubrication is essential to introduce damping forces and is given by Chaudhary and Tandon [10],

$$c_{ehl} = \frac{3\mu_0\beta_h^4}{2h_0^3} \quad (27)$$

Due to frictional losses and elastic deformation of balls, material damping comes into picture and can be calculated by the expression:

$$c_{mat} = \frac{\eta_b k_b}{2\pi f} \quad (28)$$

Damping at inner race-shaft and outer race-housing interface are considered to be hysteretic and calculated by Dietl et al.[30],

$$c_{s,h} = \frac{\eta_{s,h}K_{s,h}}{2\pi f} \quad (29)$$

2.5 Ball deformation

The i^{th} ball deformation is dependent on radial deflection and varies with its angular position. The total ball deformation is the sum of deflection at inner race and outer race.

$$\delta_i^{total} = \delta_i^{inner} + \delta_i^{outer} \quad (30)$$

were,

$$\delta_i^{inner} = (x_s - x_{bi})cos\theta_i + (y_s - y_{bi})sin\theta_i - c_r \quad (31)$$

$$\delta_i^{outer} = (x_{bi} - x_h)cos\theta_i + (y_{bi} - y_h)sin\theta_i \quad (32)$$

As the lubricant film fill the clearance in bearing, it creates negative clearance, the radial clearance c_r is set as negative to cater the influence of lubricant film.

$$c_r = c_d/2 \times (1 - sin\theta) \quad (33)$$

2.6 Defect modelling

When healthy balls rolling over defect on inner and outer race, the ball centre will have an additional deflection ε_d.

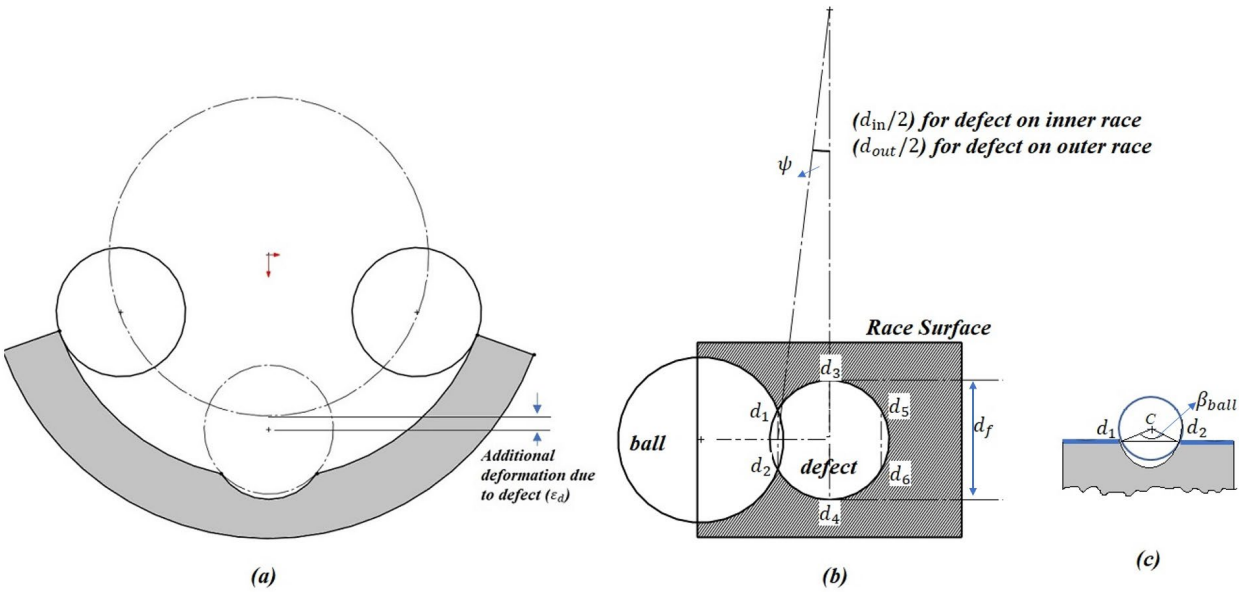

Fig. 3: Schematic diagram of ball rolling over defect on outer race (a) Front view, (b) Top view, (c) Side view

To model the expression for ε_d for this case, the geometrical analysis has been done and it is shown in Fig. 3.

From bearing geometry Fig. 3(c), the angle subtended by i^{th} ball on defect is given by,

$$\beta_{ball} = sin^{-1}\left(\frac{d_1 d_1}{d_b}\right) \quad (34)$$

were,

$$d_1 d_2 = 2 * d_1 e = \sqrt{(d_f/2)^2 - ef^2} \quad (35)$$

$$ef = (d_{out}/2)sin(\psi) \quad (36)$$

$$\varepsilon_d = \begin{cases} Min\,(H,\ \frac{d_b}{2}[1 \mp cos\,(\beta_{ball})])\,, & \alpha_d - \psi \le \theta_i \le \alpha_d + \psi \\ 0\ , & Otherwise \end{cases} \quad (37)$$

where, $0 \le \beta_{ball} \le sin^{-1}\left(\frac{d_f}{d_b}\right)$.

For inner race, the negative sign and for outer race, the positive sign is considered in expression of ε_d.

2.7 Angular positions of defects

From analysis of geometry, it can be concluded that the angular position of defect varies with time and given by

$$\alpha_d^{inner} = \omega_s t \pm \sin^{-1}(d_f/d_{in}) \quad (38)$$

$$\alpha_d^{outer} = \alpha_{dout} \pm \sin^{-1}(d_f/d_{out}) \quad (39)$$

Thus, the deformation of i_{th} ball rolling over the defect is given by,

$$\delta_i^{inner} = (x_s - x_{bi})cos\theta_i + (y_s - y_{bi})sin\theta_i - c_r - \Theta_i\varepsilon_d \quad (40)$$

$$\delta_i^{outer} = (x_{bi} - x_h)cos\theta_i + (y_{bi} - y_h)sin\theta_i - \Theta_i\varepsilon_d \quad (41)$$

where, Θ_i is a switch function.

3. Results discussion

Equations of motions (Eq. 3-8) along with angular position of balls (Eq. 1) and ball deformation (Eq. 40-41) have been solved simultaneously for step size of 10^{-7} sec time to conduct the simulation. SKF 6205 2Z bearing is adopted and vibration response of bearing system has been computed. The input parameters for bearing system are given in Table 1 and summary of results have been expressed in Table 2. The process flow adopted for computation is shown in Fig. 4.

The standard formulas to calculate the characteristic frequencies of bearing system have been used in this study.

$$BPFO = \frac{n_b\omega_s}{120}\left(1 - \frac{d_b}{D}cos\emptyset\right) \quad (42)$$

$$BPFI = \frac{n_b\omega_s}{120}\left(1 + \frac{d_b}{D}cos\emptyset\right) \quad (43)$$

Experiments have been conducted to validate the above theoretical model. The angular speed of shaft is 1482 rpm. The circular defects of 2 mm diameter are artificially created on inner race and outer race in separate bearings by electro discharge machining (EDM). The defect was positioned at 270^0 initially.

Table 1. Bearing parameters

Bearing under study	SKF 6205-2Z
Bearing Bore Diameter, (mm)	25.000
Diameter of Inner Race, (mm)	31.050
Diameter of Outer Race, (mm)	46.910
Diameter of Pitch, (mm)	38.980
Diameter of Balls, (mm)	7.930
Diametral Clearance (Cd), (µm)	10
Number of Balls	9
Ball Mass, (gm)	2.070
Inner Race Mass, (gm)	38.600
Outer Race Mass, (gm)	50.410
Shaft and Rotor Mass, (kg)	4.188
Housing Mass, (g)	216
Contact Angle (deg.)	0

A piezoelectric type STI vibration sensor with frequency range of 2 Hz to 14 kHz ±5% and sensitivity of 100mV/g ±10% is used to capture the vibration signal and DT9837B from DATATRANSLATION, a data acquisition system is used to analyze the time and frequency domain vibration signals. The actual setup is shown in Fig. 5

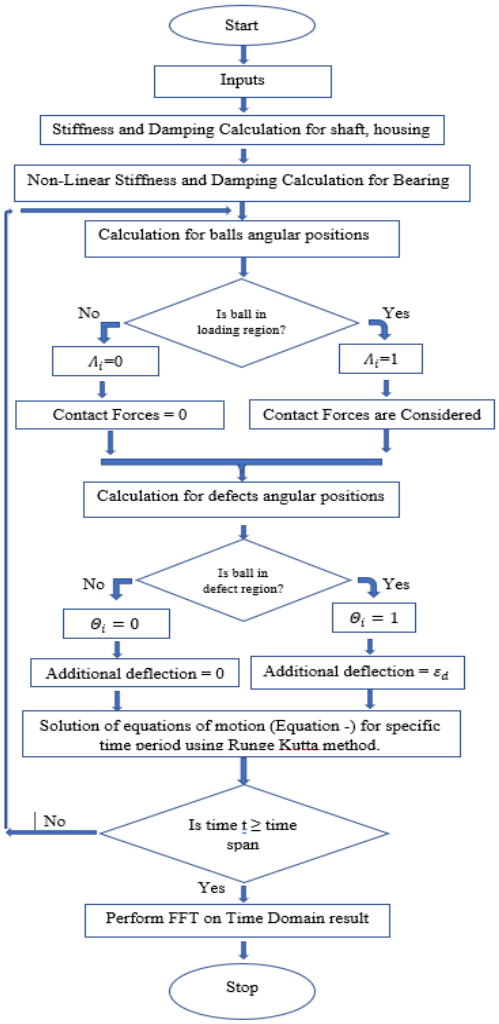

Fig. 4: Process flow diagram

Table 2. Summary of results

Condition of bearing	**Resonant frequency (Calculated)**	**Resonant frequency and velocity peak (simulated)**	**Resonant frequency and velocity peak (experimental)**
Healthy bearing	25.00 Hz	Fs=24.70 Hz Velocity peak =0.000013 mm/s	Fs = 24.88 Hz Velocity peak =0.000053 mm/s
Bearing with inner race defect	134.34 Hz	BPFI = 134.64 Hz Velocity peak = 0.000526 mm/s	BPFI = 134.38 Hz Velocity peak =0.000128 mm/s
Bearing with outer race defect	88.89 Hz	BPFO = 88.70 Hz Velocity peak = 0.000726 mm/s	BPFO = 89.01 Hz Velocity peak = 0.000062 mm/s

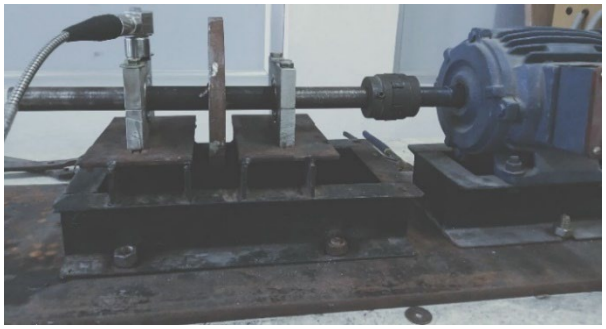

Fig. 5: Actual vibration test rig

3.1 Baseline signature of healthy bearing

Figures 6(a) and 6(b) show the simulated vibration responses in time-domain and it's enveloped frequency domain signals of housing with healthy bearing in y-direction respectively. The characteristic features visible in Figure 6(a) are due to positioning of balls in loading and non-loading zone. Due to rotation of inner race, balls spin on it and have resultant angular positions in loaded region. Due to angular positioning in loading zone, first ball start deforming and reaches maximum at $\theta = 270^0$. At this time the response of housing in Y direction shows maximum and it repeats after an interval of 0.0404 sec, which is the reciprocal of the characteristic frequency fs = 24.77 Hz.

The characteristic frequencies like cage rotational frequency fc = 9.90 Hz, shaft rotation frequency fs = 24.70 Hz are observed in Fig. 6(b).

The harmonics of shaft rotational frequency at 2*fs = 49.40 Hz, and 3*fs= 74.10 Hz, etc. are also evident.

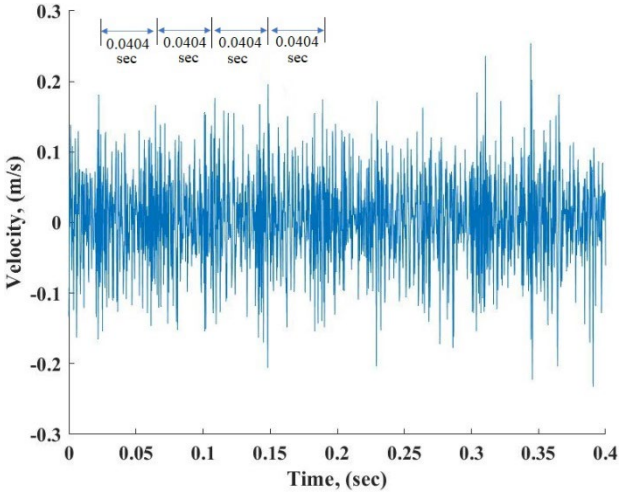

Fig. 6(a): The time-domain waveform of the simulated velocity response of housing with heathy bearing in Y direction

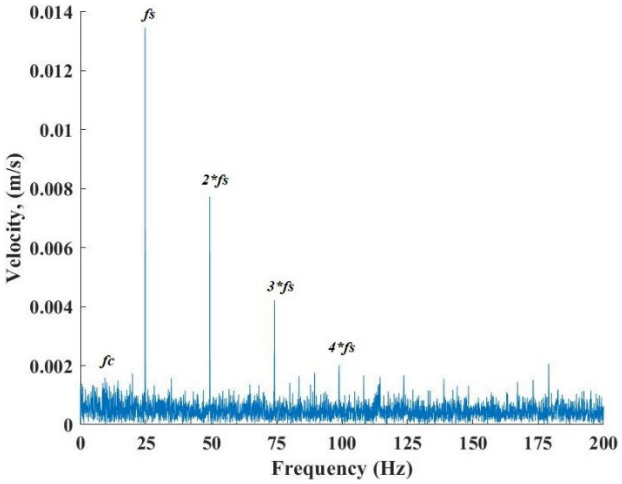

Fig. 6(b): Enveloped frequency-domain signals of simulated velocity response of housing with healthy bearing

Fig. 7 shows the experimental spectra. The characteristic frequency components as observed in simulation results are also present in the experimental results at cage rotational frequency fc=9.90 Hz, shaft rotation frequency fs = 24.88 Hz and its harmonics at 2*fs= 49.76 Hz, and 3*fs= 74.64 Hz, etc.

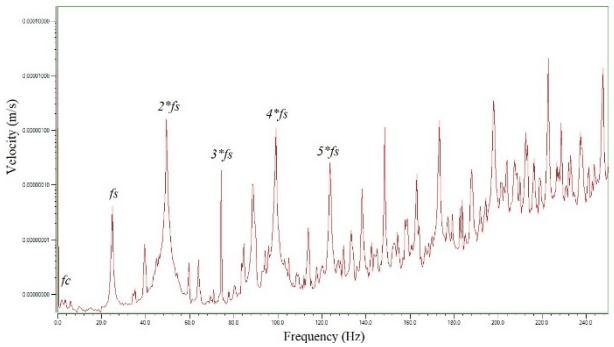

Fig. 7: Experimental velocity response of housing with healthy bearing

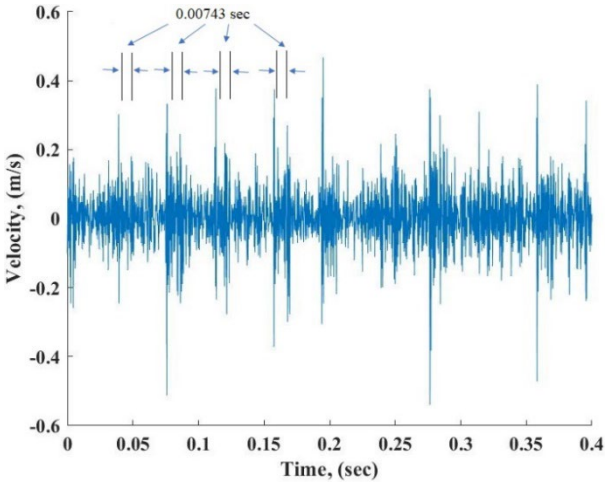

Fig. 8(a): The time-domain waveform of simulated velocity response of housing with bearing having inner race defect

3.2 Bearing with defect on inner race

The angular position of inner race defect changes with the rotation of shaft and due to this complicated vibration responses are generated.

Fig. 8(a) and Fig. 8(b) show the time-domain waveform and it's enveloped frequency-domain signals of the simulated velocity responses of housing with defect on inner race, in Y direction, respectively. The time interval between two impacts depicted in Fig. 8(a) is 0.00743 sec, and it is same in form of characteristic frequency BPFI. The characteristic frequencies are observed in Fig. 8(b) at the rotational frequency of shaft fs = 24.77 Hz and its harmonics at 2*fs= 49.54 Hz, and 3*fs= 74.31 Hz, along with BPFI = 134.54 Hz and its harmonics. In this case, due to rotation of defect with the speed of shaft, the amplitude modulation occurs in characteristic frequency BPFI. Therefore, peaks are observed at frequencies BPFI-fs = 109.70, BPFI + fs =159.32 Hz and its harmonics. The sidebands with bandwidth equal to ball rotational frequency are also present near the characteristic frequency.

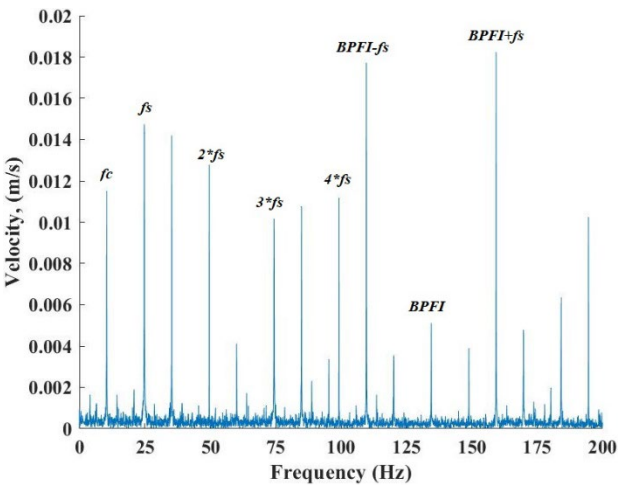

Fig. 8(b): Enveloped frequency-domain signals of simulated velocity response of housing with bearing having inner race

defect

In Fig. 9, the velocity response is captured experimentally on housing with bearing having defect on inner race. The BPFI peaks at 134.38 Hz and its harmonics, very close to simulated result at 134.64 Hz is observed. The characteristic frequencies at shaft rotational frequency fs = 24.90 Hz and its harmonics at 2*fs = 49.80 Hz, and 3*fs= 74.72 Hz are also observed. The amplitude modulated BPFI with shaft speed causes peaks at frequencies BPFI-fs = 109.48 Hz, BPFI + fs =159.28 Hz and its harmonics.

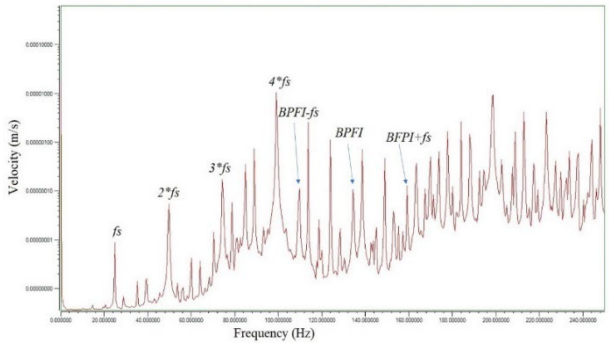

Fig. 9: Experimental velocity response of housing with bearing having inner race defect

3.3 Bearing with defect on outer race

The angular position of outer race defect is fixed and when ball rolls over defect, an impact response is produced. Fig. 10(a) and Fig. 10(b) show the time-domain waveform and it's enveloped frequency-domain signals of the simulated velocity responses of housing with defect on outer race, in Y direction, respectively. The time interval between two impacts depicted in Fig. 10(a) is 0.01126 sec, and it is same in form of characteristic frequency BPFO.

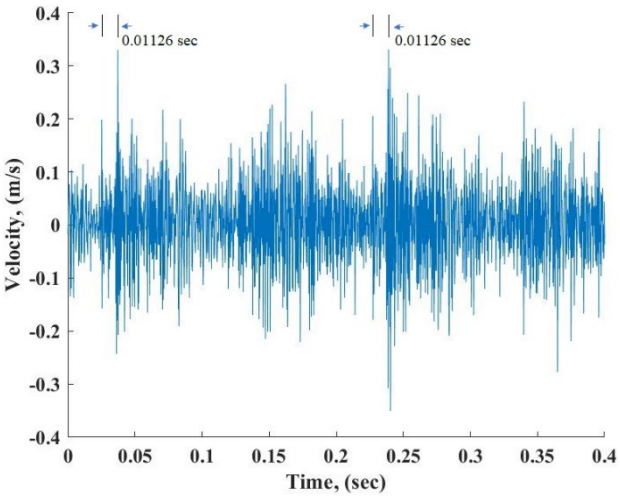

Fig. 10(a): The time-domain waveform of simulated velocity response of housing with bearing having outer race defect

The characteristic frequencies like shaft rotational frequency fs = 24.77 Hz and its harmonics at 2*fs = 49.54 Hz, and 3*fs= 74.31Hz including BPFO = 88.70 Hz and its harmonics are observed.

In Fig. 11, the velocity response is captured experimentally on housing with bearing with outer race defect. The characteristic frequencies at shaft rotation frequency fs = 24.78 Hz and its harmonics at 2*fs = 49.56 Hz, and 3*fs= 74.34 Hz along with peak at BPFO=89.01 Hz are observed which very close to the simulated results.

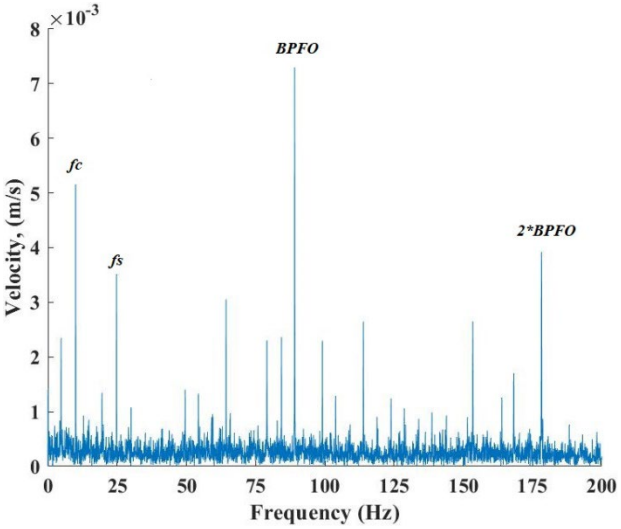

Fig. 10(b): Enveloped frequency-domain signals of simulated velocity response of housing with bearing having outer race defect

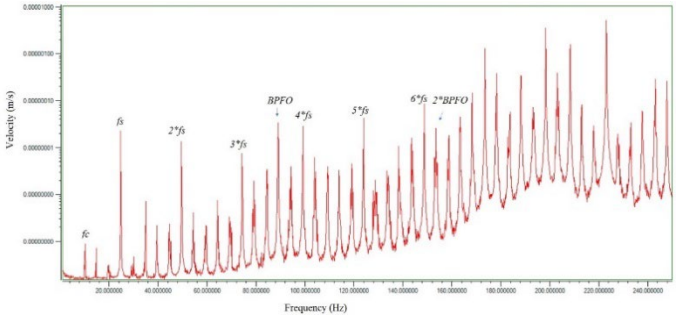

Fig. 11: Experimental velocity response of housing with bearing having outer race defect

It is evident from Table 2 that the characteristic frequencies in simulated results differ by 0.19 % to 0.72 % with experimental results which is negligible. But the velocity amplitudes at characteristic frequencies in simulated results are in poor agreement with experimental values. This is due to the defects like misalignment, residual unbalancing, etc. are ignored in the theoretical model.

4. Conclusion

The vibration model, to analyze the local defect in deep groove ball bearing system is developed. Shaft,

races, balls and housing masses along with damping at ball-race interface and defects on its races are considered in the model. The governing equations are solved using MATLAB to simulate the vibration responses of bearing system. To validate the simulation results, experiments have been conducted and experimental results are compared with simulated results. Peaks at shaft rotational frequency, cage frequency along with their harmonics, BPFI and its amplitude modulation with shaft rotational frequencies along with their harmonics and BPFO along with their harmonics are clearly evident in vibration responses of bearing system. The comparison in Table 2 shows that the characteristic frequencies in simulated results differ by 0.19 % to 0.72 % with experimental results which is negligible. But the velocity amplitudes at characteristic frequencies in simulated results are in poor agreement with experimental values. This is due to the defects like misalignment, residual unbalancing, etc. are ignored in the theoretical model. Since the simulated results are depicting the same characteristics as it is shown in experimental results, therefore, this vibration model can be used to study the vibration characteristics and to predict the localized defects in ball bearings.

Acknowledgements

Ajay Kumar Verma, acknowledge and thank the management of Shivalik College of Engineering, Dehradun for permitting and providing the infrastructural support to pursue PhD at NIT Kurukshetra.

Nomenclature

c_b	coefficient of damping of bearing (Ns/mm)
c_h	coefficient of damping of housing (Ns/mm)
c_{ehl}	coefficient of damping due to elstohydrodynamic lubrication (Ns/mm)
c_s	coefficient of damping of shaft (Ns/mm)
c_{mat}	coefficient of damping of material (Ns/mm)
c_r	radial clearance (mm)
d_b	diameter of ball (mm)
d_f	diameter of defect (mm)
d_{in}	diameter of inner race (mm)
d_{out}	diameter of outer race (mm)
D	pitch circle diameter of bearing (mm)
E	Young's modulus, (mm)
f_c	contact force at ball-races interface (N)
f_d	damping force (N)
H	spall height (mm)
k_b	contact stiffness of bearing (N/mm^3)
k_h	stiffness of housing (N/mm)
k_s	stiffness of shaft (N/mm)
m_b	mass of ball (g)
m_h	mass of housing (kg)
m_s	mass of shaft (kg)
n_b	number of balls
R	radius of curvature (mm)
x	deflection along x-axis (mm)
y	deflection along y-axis (mm)

Greek symbols

α_d	angular position of defect with reference to x-axis
β_{ball}	angle subtended by defect with reference to ball centre (rad)
ψ	angle subtended by defect with reference to bearing centre (rad)
$\sum\rho$	curvature sum (mm)
v	Poisson's ratio
η	loss factor
ε_d	additional deflection of ball due to defect (mm)
ω_{cage}	angular speed of cage (rad/sec)
ω_s	angular speed of shaft (rad/sec)
θ_i	angular position of ith ball with reference to x-axis (rad)
δ_i	deformation of ith ball (mm)
ϕ	contact angle of ball in bearing (rad)

References

1) N. Tandon, and A. Choudhury, "Review of vibration and acoustic measurement methods for the detection of defects in rolling element bearings", *Tribol. Int.,* **32**, 469–480 (1999). doi: 10.1016/S0301-679X(99)00077-8
2) M. S. Patil, J. Mathew, and P. K. R. Kumar, "Bearing signature analysis as a medium for fault detection: A review", *J. Tribol.,* **130**, 1–7 (2008). doi: 10.1115/1.2805445
3) S. Fukata, E.H. Gad, T. Kondou, T. Ayabe, and H. Tamura, "On the radial vibrations of ball bearings (computer simulation)", *Bulletin of the JSME,* **28**, 899–904 (1985). doi: 10.1299/jsme1958.28.899
4) P. D. McFadden, and J.D. Smith, "The vibration produced by multiple point defects in a rolling element bearing", *J. Sound Vib.,* **98**, 263–273 (1985). doi: 10.1016/0022-460X(85)90390-6
5) P. D. McFadden, and J.D. Smith, "Model for the vibration produced by a single point defect in a rolling element bearing", *J. Sound Vib.,* **96**, 69–82 (1984). doi: 10.1016/0022-460X(84)90595-9
6) N. Tandon, and A. Choudhury, "An Analytical Model for the Prediction of the Vibration Response

of Rolling Element Bearings Due to Localized Defect", *J. Sound Vib.*, **205**, 275–292 (1997). doi: 10.1006/jsvi.1997.1031

7) M. Tiwari, K. Gupta, and O. Prakash, "Effect of radial internal clearance of a ball bearing on the dynamics of a balanced horizontal rotor", *J. Sound Vib.*, **238**, 723–756 (2000). doi: 10.1006/jsvi.1999.3109
8) M. Tiwari, K. Gupta, and O. Prakash, "Dynamic response of an unbalanced rotor supported on ball bearings", *Journal of Sound and Vibration*, **238**, 757–779 (2000). doi: 10.1006/jsvi.1999.3108
9) N. S. Feng, E. J. Hahn, and R. B. Randall, "Using transient analysis software to simulate vibration signals due to rolling element bearing defects", *Proceedings of the 3rd Australian Congress on Applied Mechanics, Sydney, Australia*, (2002). doi: 10.1142/9789812777973_0112
10) A. Choudhury, and N. Tandon, "Vibration response of rolling element bearings in a rotor bearing system to a local defect under radial load", *J. Tribol.*, **128**, 252–261 (2006). doi: 10.1115/1.2164467
11) Z. Kiral, and H. Karagülle, "Vibration analysis of rolling element bearings with various defects under the action of an unbalanced force", *Mech. Syst. Signal Process,* **20**, 1967–1991 (2006). doi: 10.1016/j.ymssp.2005.05.001
12) F. Cong, J. Chen, G. Dong, and M. Pecht, "Vibration model of rolling element bearings in a rotor-bearing system for fault diagnosis", *Journal of Sound and Vibration*, **332**, 2081– 2097 (2013). doi: 10.1016/j.jsv.2012.11.029
13) H. Arslan, and N. Aktürk, "An investigation of rolling element vibrations caused by local defects", *J. Tribol.,* **130**, 1–12 (2008). doi: 10.1115/1.2958070
14) D. Brie, "Modeling of the Spalled Rolling Element Bearing Vibration Signal: An Overview and Some New Results", *Mech. Syst. Signal Process*, **14**, 353–369 (2000). doi: 10.1006/mssp.1999.1237
15) N. Tandon, and B. C. Nakra, "Detection of Defects in Rolling Element Bearings by Vibration Monitoring", J. Inst. Eng. India, Mechanical Engineering Division, **73**, 271–282 (1993). doi: 10.1108/02656719210010721
16) N. Tandon, "A comparison of some vibration parameters for the condition monitoring of rolling element bearings", *Measurement*, **12**, 285–289 (1994). doi: 10.1016/0263-2241(94)90033-7
17) A. Ashtekar, F. Sadeghi, and L. E. Stacke, "A new approach to modeling surface defects in bearing dynamics simulations", *J. Tribol*., **130**, 1–8 (2008). doi: 10.1115/1.2959106
18) J. Sopanen, and A. Mikkola, "Dynamic model of a deep-groove ball bearing including localized and distributed defects", Part 1: Theory, *Proc. Inst*., **217**, 201–211 (2003). doi: 10.1243/14644190360713551
19) J. Sopanen, and A. Mikkola, "Dynamic model of a deep-groove ball bearing including localized and distributed defects. Part 2: Implementation and results", *Proc. Inst. Mech. Eng. Part K J. Multi Body Dyn.,* **217**, 213–223 (2003). doi: 10.1243/14644190360713560
20) Y. H. Wijnant, J. A. Wensing, and G. C. V. Nijen, "The influence of lubrication on the dynamic behaviour of ball bearings", *Journal of Sound and Vibration*, **222**, 579–596 (1999). doi: 10.1006/jsvi.1998.2068
21) C. K. Babu, N. Tandon, and R. K. Pandey, "Vibration modeling of a rigid rotor supported on the lubricated angular contact ball bearings considering six degrees of freedom and waviness on balls and races", *J. Vib. Acoust. Trans., ASME*, **134**, 1–12 (2012). doi: 10.1115/1.4005140
22) G. Yu, M. Su, W. Xia, R. Wu, and Q. Wang, "Vibration characteristics of deep groove ball bearing based on 4-DOF mathematical model", *Procedia Engineering*, **174**, 808– 814, (2017). doi: 10.1016/j.proeng.2017.01.226
23) P. Hou, L. Wang, and Q. Peng, "Vibration analysis of ball bearing considering waviness under high speed and an axial load", *BULLETIN OF THE POLISH ACADEMY OF SCIENCES TECHNICAL SCIENCES*, **68** (03), 517-527, (2020). doi:10.24425/bpasts.2020.133382
24) X. Zhang, C. Yan, Y. Liu, P. Yan, Y. Wang, and Lixiao Wu, "Dynamic Modeling and Analysis of Rolling Bearing with Compound Fault on Raceway and Rolling Element", *Shock and Vibration, Special Issue*, **2020**, 1-16, (2020). doi:10.1155/2020/8861899
25) X. Gao, C. Yan , Y. Liu, P. Yan, J. Yang and L. Wu, "A 4-DOF dynamic model for ball bearing with multiple defects on raceways", *Proc. IMechE Part K: J Multi-body Dynamics*, **235**(1), 3–18, (2021). doi:10.1177/1464419320972870
26) F. Li, X. Li and D. Shang, "Dynamic Modeling and Vibration Characteristics Analysis of Deep-Groove Ball Bearing, Considering Sliding Effect", *Mathematics*, **2408**(9), 1-16, 2021. doi:10.3390/math9192408
27) T. A. Harris, "*Introduction to Rolling Bearings*", **3**, John Wiley & Sons, New York, (1991).
28) D. E. Brewe, and B. J. Hamrock, "Simplified solution for elliptical-contact deformation between two elastic solids", *J. Lubrication Technol.*, **99**, 485–487 (1977). doi: 10.1115/1.3453245

29) S.P. Harsha, K. Sandeep, and R. Prakash, “Non-linear dynamic behaviors of rolling element bearings due to surface waviness”, *J. Sound Vib.,* **272**, 557–580 (2004).
doi: 10.1016/S0022-460X(03)00384-5
30) P. Dietl, J. Wensing, and G.C. Van Nijen, “Rolling bearing damping for dynamic analysis of multi-body systems - Experimental and theoretical results,” *Proc. Inst. Mech. Eng. Part K J. Multi-Body Dyn.,* **214**, 33–43 (2000).
doi: 10.1243/1464419001544124
31) S. K. Lambha, V. Kumar, and R. Verma, “Performance Characteristics of a Deformed 120-Degree Partial Bearing with Couple Stress Lubrication”, *EVERGREEN Joint Journal of Novel Carbon Resource Sciences & Green Asia Strategy*, **09** (02), 269-282, (2022)
doi: 10.5109/4793662
32) A. C. Opia, M. K. A. Hamid, S. Syahrullail, A. I. Ali, C. N. Johnson, I. Veza, M. I. Izmi, C. D. Z. Hilmi, and A. B. A. Rahim, “Tribological Behavior of Organic Anti-Wear and Friction Reducing Additive of ZDDP under Sliding Condition: Synergism and Antagonism Effect”, *EVERGREEN Joint Journal of Novel Carbon Resource Sciences & Green Asia Strategy*, **09**(02), 246-253, (2022).
doi: 10.5109/4793628
33) A. C. Opia, M. K. A. Hamid, S. Syahrullail, C. A. N. Johnson, A. B. Rahim, and M. B. Abdulrahman, “Nano-Particles Additives as a Promising Trend in Tribology: A Review on their Fundamentals and Mechanisms on Friction and Wear Reduction”, *EVERGREEN Joint Journal of Novel Carbon Resource Sciences & Green Asia Strategy*, **08**(04), 777-798, (2021)
doi: 10.5109/4742121
34) Safril, Mustofa, M. Zen, F. Sumasto, and M. Wirandi, "Design of Cooling System on Brushless DC Motor to Improve Heat Transfers Efficiency", *EVERGREEN Joint Journal of Novel Carbon Resource Sciences & Green Asia Strategy*, **09**(02), 584-593, (2022).
doi:10.5109/4794206
35) P. Gupta, B. Singh, and Y. Shrivastava, " Robust Techniques for Signal Processing: A Comparative Study", *EVERGREEN Joint Journal of Novel Carbon Resource Sciences & Green Asia Strategy*, **09**(02), 404-411, (2022).
doi:10.5109/4794165